THE JOURNAL OF PHYSICAL CHEMISTRY B

Article

pubs.acs.org/JPCB

Protein Dynamics in the Solid State from ^{2}H NMR Line Shape Analysis. II. MOMD Applied to C−D and C−CD_3 Probes

Eva Meirovitch,*[,†] Zhichun Liang,[‡] and Jack H. Freed*[,‡]

[†]The Mina and Everard Goodman Faculty of Life Sciences, Bar-Ilan University, Ramat-Gan 52900, Israel

[‡]Baker Laboratory of Chemistry and Chemical Biology, Cornell University, Ithaca, New York 14853-1301, United States

ABSTRACT: Deuterium line shape analysis from mobile C−D and C−CD_3 groups has emerged as a particularly useful tool for studying dynamics in the solid state. The theoretical models devised so far consist typically of sets of independent dynamic modes. Each such mode is simple and usually case-specific. In this scenario, model improvement entails adding yet another mode (thereby changing the overall model), comparison of different cases is difficult, and ambiguity is unavoidable. We recently developed the microscopic order macroscopic disorder (MOMD) approach as a single-mode alternative. In MOMD, the local spatial restrictions are expressed by an anisotropic potential, the local motion by a diffusion tensor, and the local molecular geometry by relative (magnetic and model-related) tensor orientations, all of adjustable symmetry. This approach provides a consistent method of analysis, thus resolving the issues above. In this study, we apply MOMD to PS-adsorbed LKα14 peptide and dimethylammonium tetraphenylborate (C−CD_3 and N−CD_3 dynamics, respectively), as well as H*ha*I methyltransferase target DNA and phase III of benzene-6-hexanoate (C−D dynamics). The success with fitting these four disparate cases, as well as the two cases in the previous report, demonstrates the generality of this MOMD-based approach. In this study, C−D and C−CD_3 are both found to execute axial diffusion (rates $R_\perp$ and $R_\parallel$) in the presence of a rhombic potential given by the $L = 2$ spherical harmonics (coefficients c_0^2 and c_2^2). $R_\perp$ ($R_\parallel$) is in the 10^2−10^3 (10^4−10^5) s^{-1} range, and c_0^2 and c_2^2 are on the order of 2−3 k_BT. Specific parameter values are determined for each mobile site. The diffusion and quadrupolar tensors are tilted at either 120° (consistent with *trans*−*gauche* isomerization) or nearly 110.5° (consistent with methyl exchange). Future prospects include extension of the MOMD formalism to include MAS, and application to ^{15}N and ^{13}C nuclei.

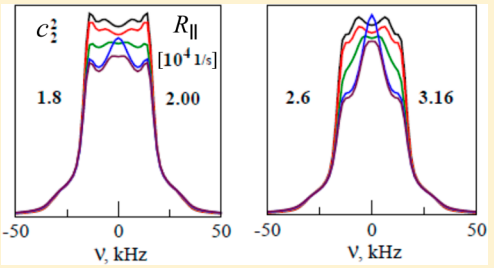

1. INTRODUCTION

^{2}H NMR line shape analysis is a powerful method for studying structural dynamics in the solid state.[1,2] The [isopropyl-$^2H_7$]-leucine probe has been used in early work to investigate the dynamics of collagen fibrils.[3] In recent years, this probe has been used to study physisorption of the Ac-LKKLLKLLKKLLKL-OH (LKα14) peptide onto polystyrene (PS) and PS-COOH surfaces and carboxyl-functionalized gold nanoparticles.[4−6] The d_3-alanine and d_3-leucine probes have been used to investigate the dynamics of phospholamban embedded in phospholipid bilayers,[7,8] as well as partitioning and orientation of the lung surfactant peptide KL4 in phospholipid bilayers.[9] The probes d_3-leucine and d_8-valine have been used recently to study side-chain dynamics in the core of the Chicken Villin Headpiece Subdomain (HP36).[10,11] Extensive work associated with lipids, peptides, and proteins has been carried out by the groups of Seelig (e.g., ref 12), Davis (e.g., ref 13), Griffin (e.g., ref 14), Oldfield (e.g., ref 15), Brown (e.g., ref 16), etc. Deuterated tyrosine side chains have served as a probe for studying peptide dynamics (e.g., ref 17). ^{2}H-Labeled methylene groups have been used to study polymer dynamics (e.g., ref 18). Deuterium NMR has been used extensively to study liquid crystals.[19−21] Work focusing on NMR line shape and relaxation analysis in solids, where key aspects have been treated, is described in refs 22−25. We also contributed in the past to this field of research.[17,26−28]

Traditionally, dynamics in the solid-state have been envisioned as jump-type motions associated with barrier-crossing and hops among energy wells (e.g., ref 29). Only when the activation energy turned out to be very small were simple diffusive models developed and utilized (e.g., ref 30). However, a single (typically jump-type) simple motion often does not reproduce satisfactorily dynamic ^{2}H line shapes in the solid state. Rather, several independent simple motions have to be combined (e.g., refs 4−6, 10, and 11). These multi-simple-mode models are typically case-specific; hence, comparison among different systems is difficult. In this scenario, the agreement between calculated and experimental spectra can only be improved by adding yet another simple mode; this alters the overall model. Finally, the multi-simple-mode concept is inherently ambiguous, as many different combinations of simple motions are possible.

No model can be proven to be unique. However, a general and comprehensive approach to the treatment of restricted motions has been developed within the scope of the stochastic

Received: July 31, 2015
Revised: September 21, 2015
Published: September 24, 2015

DOI: 10.1021/acs.jpcb.5b07434
J. Phys. Chem. B 2015, 119, 14022−14032

Liouville equation (SLE) by Freed and co-workers. The SLE applies to restricted overall[31−35] as well as internal[36−38] motions. The major underlying factors—type of motion, spatial restrictions, and geometry—are treated generally for the entire motional range, within their rigorous three-dimensional tensorial requirements.

Particularly relevant in the present context is the extension of the SLE called microscopic-order-macroscopic-disorder (MOMD) approach, where the director of the restricting environment is distributed randomly over the sample.[39] MOMD/ESR was applied to nitroxide probes in liposomes,[40] and later to internal motions in nitroxide-labeled proteins and DNA fragments in "frozen" solutions (i.e., scenarios where the global motion of the (typically large) molecule may be considered "frozen" on the ESR time scale).[41,42] The ESR nitroxide label in "frozen" solutions is formally analogous to the NMR ^{2}H label in polycrystalline proteins. In MOMD, parameter combinations differing in complexity can be devised by monitoring tensor magnitude, symmetry, and orientation.[39] This enables a continuous range of scenarios, and thus comparison among different systems, within the scope of the same general model. Thereby, the problematic issues associated with previous ^{2}H line shape analyses (see above) are expected to be largely resolved.

On the basis of this reasoning, we recently developed MOMD[39] for the analysis of dynamic ^{2}H NMR line shapes.[43] Our approach was applied to C−CD_3 dynamics in HP36 and an example of S−CD_3 dynamics in the *Streptomyces* Subtilisin Inhibitor (SSI).[43] The emerging physical picture depicts the spin-bearing probe executing axially symmetric diffusion (with rate constants $R_\perp$ and $R_\parallel$) in the presence of a rhombic local potential given by the $L = 2$ and $K = 0$, 2 spherical harmonic functions (with coefficients c_0^2 and c_2^2). The axial diffusion frame, M, is tilted from the axial quadrupolar tensor frame, Q, at 120° or nearly 110.5° (angle β_{MQ}). The physical processes consistent with these geometric features are *trans*−*gauche* isomerization and methyl exchange, respectively. The uncertainty of the results has been estimated at 10% for c_0^2 and c_2^2, 15% for the motional rates, and 3% for the angle β_{MQ}.[43]

It is important to apply MOMD to additional systems differing in nature to test its generality. Also, one should determine whether the parameter combination delineated above is appropriate in all cases. If it is not, adequate parameter combinations need to be devised. It is, in addition, insightful to compare MOMD analyses of different systems. Finally, it is of interest to compare the MOMD-based pictures with the corresponding multi-simple-mode-based pictures.

These are the objectives of the present study. Along these lines, we apply MOMD to C−CD_3 dynamics in the PS-adsorbed LKα14 peptide[4] and in dimethylammonium tetraphenylborate.[44] In addition, we apply MOMD to C−D dynamics in the furanose ring of H*ha*I methyltransferse target DNA[30] and benzene-6-hexanoate in phase III.[45] The parameter combination found suitable to describe ^{2}H dynamics in HP36 and SSI is also found suitable for describing ^{2}H dynamics in the systems investigated in this work. The quantitative analysis reveals interesting new system-specific information.

The six different cases treated so far (four in this work and two in the study where the MOMD/NMR was developed[43]) demonstrate the benefit and power of model generality. Future prospects of this work include incorporation of magic angle spinning in the MOMD formalism, application to ^{15}N and ^{13}C nuclei, and further generalization of the MOMD model.

MOMD[39,43] represents the limit of the two-body coupled-rotator slowly relaxing local structure (SRLS) approach[36−38] where the slow rotator is "frozen", yielding random orientations of the local director. In recent years, we applied SRLS to NMR relaxation from proteins in aqueous solution.[46−50] Thus, the same general physically relevant theoretical/computational tool is now available for studying protein dynamics in the solid and liquid states.

A theoretical summary is provided in section 2. Results and discussion are summarized in section 3. Our conclusions appear in section 4.

2. THEORETICAL SUMMARY

The MOMD theory as applied to NMR has been delineated in ref 43. A brief summary is given below. Figure 1 shows the MOMD frame scheme for a deuterium nucleus. L is the space-fixed laboratory frame. C is the local director frame fixed in the molecule. M denotes the principal axes system (PAS) of the local ordering tensor, **S**, taken the same (for simplicity) as the PAS of the local diffusion tensor, **R**. Q denotes the PAS of the quadrupolar tensor. The M and Q frames are fixed in the probe.

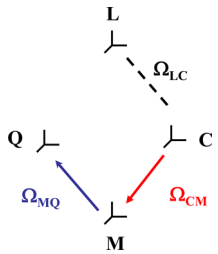

Figure 1. MOMD frames: L - lab frame, C - local director frame, M - PAS of the local ordering/local diffusion tensor, Q - PAS of the quadupolar tensor, **Q**, or the partially averaged-by-methyl-rotation quadrupolar tensor, ⟨**Q**⟩. The Euler angles Ω_{MQ} are fixed. The Euler angles Ω_{CM} are time-dependent. ^{2}H NMR spectra are calculated for every Ω_{LC} and convoluted according to a random distribution.[43]

The Euler angles Ω_{CM} (associated with the orientation and diffusion of the probe relative to the local director) are time-dependent. The Euler angles $\Omega_{MQ} = (\alpha_{MQ}, \beta_{MQ}, \gamma_{MQ})$ are time-independent. Given that the Q frame is axially symmetric, one has $\gamma_{MQ} = 0$. For simplicity, the angle α_{MQ} is set equal to zero. Thus, the orientation of Z_M (main ordering/diffusion axis) relative to Z_Q (the known principal axis of the quadrupolar tensor, or the partially averaged-by-methyl-rotation quadrupolar tensor) is given by the polar angle, β_{MQ}. Since there is no "macroscopic order", one has to calculate ^{2}H spectra for every Ω_{LC}, and convolute the corresponding line shapes according to a random distribution.[43]

The stochastic Liouville equation (SLE) for the spin density matrix is given by[31−43]

$$\left(\frac{\partial}{\partial t}\right)\rho(\Omega, t) = [-i\mathcal{H}(\Omega)^X - \Gamma_\Omega]\rho(\Omega, t), \quad \text{with } \Gamma_\Omega P_0(\Omega) = 0 \tag{1}$$

$\mathcal{H}(\Omega)^X$ is the superoperator for the orientation-dependent spin Hamiltonian. Γ_Ω is a Markovian operator for the rotational reorientation of the spin-bearing moiety (probe), with the Euler angles $\Omega \rightarrow (\alpha, \beta, \gamma)$ (Ω_{CM} in the notation above) representing the orientational angles. $P_0(\Omega)$ is the unique equilibrium probability distribution of Γ_Ω.

DOI: 10.1021/acs.jpcb.5b07434
J. Phys. Chem. B 2015, 119, 14022−14032

A simple form of the diffusion operator, Γ_Ω, is[31]

$$-\Gamma_\Omega = R\nabla_\Omega{}^2 P(\Omega, t) - (R/k_BT)(\sin\beta)^{-1}\partial/\partial\beta[\sin\beta TP(\Omega, t)] \quad (2)$$

where R is the isotropic rotational diffusion rate, $\nabla_\Omega{}^2$ is the rotational diffusion operator in the Euler angles, Ω, and T is the restoring torque. The latter is equal to $\partial u/\partial\beta$ for an axial restoring potential, e.g., $u \cong -^3/_2 c_0^2(\cos\beta)^2$ (the coefficient c_0^2 is given in units of k_BT). The expression of Γ_Ω for rhombic diffusion tensor and rhombic potential is given in ref 32.

In this study, we are using an axial diffusion tensor, R, associated in the absence of a restricting potential with three decay rates, $\tau_K^{-1} = 6R_\perp + K^2(R_\parallel - R_\perp)$, where $K = 0$, 1, and 2 (K is the order of the rank 2 diffusion tensor). $R_\parallel$ and $R_\perp$ are the principal values of $\mathbf{R}$; one may also define $\tau_\parallel = 1/(6R_\parallel)$ and $\tau_\perp = 1/(6R_\perp)$.

For a uniaxial local director, one may expand the potential in the complete basis set of the Wigner rotation matrix elements, $D^L_{0,K}(0, \theta, \varphi)$, which are proportional to the spherical harmonics. One has[32]

$$u(\theta, \varphi) = -\sum_{L=1}^{\infty}\sum_{K=-L}^{+L} c_K^L D^L_{0,K}(0, \theta, \varphi) \quad (3)$$

with $u(\theta, \varphi)$ and c_K^L being dimensionless. If only the lowest, $L = 2$, terms are preserved, one obtains the real potential:[32,39]

$$u(\Omega_{CM}) \approx -c_0^2 D^2_{0,0}(\Omega_{CM}) - c_2^2[D^2_{0,2}(\Omega_{CM}) + D^2_{0,-2}(\Omega_{CM})] \quad (4)$$

with c_0^2 evaluating potential strength and c_2^2 potential rhombicity. This form of $u(\Omega_{CM})$ is used herein.[43]

Local order parameters are defined as[32]

$$\langle D^2_{0,K}(\Omega_{CM})\rangle = \int d\Omega_{CM} D^2_{0,K}(\Omega_{CM}) \exp[-u(\Omega_{CM})]/\int d\Omega_{CM} \exp[-u(\Omega_{CM})], \quad K = 0, 2 \quad (5)$$

For at least 3-fold symmetry around the local director, C, and at least 2-fold symmetry around the principal axis of the local ordering tensor, Z_M, only $S_0^2 \equiv \langle D^2_{0,0}(\Omega_{CM})\rangle$ and $S_2^2 \equiv \langle D^2_{0,2}(\Omega_{CM}) + D^2_{0,-2}(\Omega_{CM})\rangle$ survive.[32] The Saupe scheme order parameters relate to irreducible tensor components, S_0^2 and S_2^2, as $S_{xx} = ((3/2)^{1/2}S_2^2 - S_0^2)/2$, $S_{yy} = -((3/2)^{1/2}S_2^2 + S_0^2)/2$, and $S_{zz} = S_0^2$.

The diffusion operator of eq 2 comprises the rate constant R (principal value of the isotropic diffusion tensor) and the parameter c_0^2 (coefficient of the axial potential). The (enhanced) diffusion operator used in this study comprises the rate constants $R_\perp$ and $R_\parallel$ (principal values of the axial diffusion tensor) and the parameters c_0^2 and c_2^2 (coefficients of the rhombic potential). The diffusion operator Γ_Ω is given in the M frame; the superoperator $\mathcal{H}(\Omega)^X$ is given in the Q frame. Therefore, in solving the SLE (eq 1), one has to convert the M frame into the Q frame. This is accomplished by the Wigner rotation based on the angle β_{MQ}.

The solution of the SLE (eq 1), with the appropriate forms of Γ_Ω and $P_0(\Omega)$, and the specified values of Q (quadrupole constant), c_0^2, c_2^2, $R_\perp$, $R_\parallel$, and β_{MQ}, represents the calculated MOMD spectrum.

3. RESULTS AND DISCUSSION

The parameters c_0^2, c_2^2, $R_\parallel$, and $R_\perp$ are allowed to vary in the data-fitting process; the angle β_{MQ} is fixed as delineated below.

3.1. General Assessments. *Local Spatial Restrictions.* In our recent application of MOMD to C−CD_3 dynamics of leucine residues of HP36 and S−CD_3 dynamics of a methionine residue of SSI, we determined c_0^2 and c_2^2 to be approximately 2−3 k_BT.[43] ^{2}H line shapes from C2′−$^2H_2$ in *Hha*I methyltransferase target DNA have been used in previous work to study furanose ring dynamics.[30] The local spatial restrictions have been expressed in terms of an *axial* potential, the coefficient of which has been determined to be approximately 5 k_BT.

The dominant simple mode associated with C−D and C−CD_3 dynamics is two-site exchange.[3−6,10,11,14,44,45] In this process, the population ratio, p_1/p_2, represents implicitly the spatial restrictions (favoring one conformer over the other). p_1/p_2 was found to range from 3/7 to 4/6 in ref 4, from 2/8 to 3.8/6.2 in ref 5, and from 2/8 to 1 in ref 45. In the extreme motional narrowing limit, one has $1/T_2 = \delta^2 \times (p_1 \times p_2)/k_{ex}$ (δ, separation between chemical shifts; k_{ex}, exchange rate). For a rigid particle reorienting diffusively in a strong potential given by $u = -c_0^2 D^2_{0,0}$, one has in the extreme motional narrowing limit $1/T_2 = \Delta^2 \times (S_0^2)^2 \times \tau$ (Δ, anisotropic magnetic interaction; $S_0^2 = \langle D^2_{0,0}\rangle$, axial order parameter; τ, diffusive correlation time). In this limit, $p_1 \times p_2$ and $(S_0^2)^2$ may be considered to be formally analogous. The p_1/p_2 values depicted above correspond to $S_0^2 = 0.45-0.63$, which in turn correspond[46] to $c_0^2 = 2-3$ k_BT.

Thus, for C−D and C−CD_3 dynamics in the system investigated in this work, the coefficients c_0^2 and c_2^2 of the MOMD potentials are most likely on the order of 2−3 k_BT.

Local Motion. The multimode models yielded exchange rates on the order of 5×10^2 to 5×10^6 (10^3-10^6) s^{-1} for C−D (C−CD_3 with spinning methyl group) dynamics. This is expected on the basis of $Q \sim 170$ kHz for C−D and $\langle Q\rangle \sim 50$ kHz ($\sim[1.5\cos^2(110.5°) - 0.5] \times 170$, where 110.5° is the tetrahedral angle corresponding to $r_{CH} = r_{CD} = 1.115$ Å)[43] for C−CD_3. In our previous application of MOMD to HP36 and SSI, we found that $R_\perp$ is quite close to its rigid limit, whereas $R_\parallel$ is moderate to fast on the dynamic C−CD_3 time scale.[43] Whether $R_\perp$ and $R_\parallel$ of other cases of C−CD_3 dynamics, and instances of C−D dynamics, exhibit similar patterns is to be determined.

Note that $R_\perp$ and $R_\parallel$ are geometrically related principal values of an axial diffusion tensor, R, the orientation of which is given by β_{MQ}. If necessary, the symmetry of R can be lowered (i.e., $R_{xx} \neq R_{yy}$), and its orientation specified by α_{MQ} and β_{MQ}. The form of the local potential (eq 4), hence the complexity (in terms of magnitude, symmetry, and orientation) of the local ordering tensor, can also be enhanced. The single-mode description will still be in effect. Within such a broad scope, implied by the tensorial representation of the physical quantities, it is not necessary to resort to multimode descriptions (which, in principle, can be implemented in MOMD).

Local Geometry. The geometric feature of particular interest is the orientation of Z_M relative to Z_Q, given by β_{MQ}. MOMD describes axial diffusive motion in the presence of a rhombic potential, rather than simple (jump-type) motions.[43] However, from a geometric point of view, one may relate β_{MQ} to geometric features associated with relevant simple motions, and view MOMD as enhanced versions of those motions.

DOI: 10.1021/acs.jpcb.5b07434
J. Phys. Chem. B 2015, 119, 14022−14032

Figure 2A illustrates *trans (left)−gauche (right)* isomerization in a polymethylene chain segment.[S1] It can be seen that the

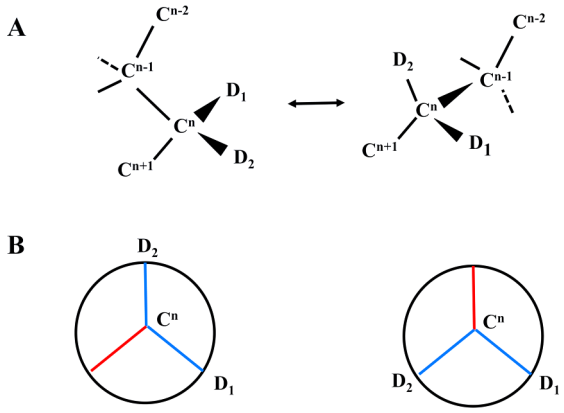

Figure 2. *Trans (left)−gauche (right)* isomerization illustrated for a polymethylene chain segment. D_1 and D_2 denote the interconverting deuterium atoms (part A). Projection along the C^n-C^{n-1} bond of the *trans* and *gauche* configurations, illustrating the angular minimum of 120° for the isomerization process. From the perspective of MOMD, the blue axes denote Z_Q, the red axis denotes Z_M, and β_{MQ} is equal to 120° (part B).

deuterium atom D_1 in the *gauche* configuration assumes the orientation originally occupied by the deuterium atom D_2 in the *trans* configuration. The configurational projection along the C^n-C^{n-1} bond (Figure 2B) illustrates the angular minimum of 120° for (jump-type) *trans−gauche* isomerization. From the perspective of MOMD, the blue axes denote Z_Q, the red axis denotes Z_M, and β_{MQ} describes their relative orientation. Thus, β_{MQ} = 120° is a physically plausible option for C−D dynamics.

Figure 3 illustrates methyl exchange between two out of the four corners of the carbon tetrahedron.[4] Within the scope of

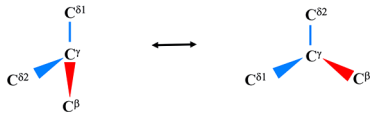

Figure 3. Methyl jumps between two out of the four corners of the carbon tetrahedron, involving an angular change of 110.5°. From the perspective of MOMD, the blue axes denote Z_Q, the red axis denotes Z_M, and β_{MQ} is equal to 110.5°.

this process, Z_M (red) is tilted at 110.5° from Z_Q (blue). Thus, β_{MQ} = 110.5° is a physically plausible option for $C-CD_3$ dynamics.

In fitting the experimental data, we set first β_{MQ} equal to 110.5 or 120°. If both values yield physically relevant and statistically appropriate (i.e., acceptable) results, the alternative with the better statistics will be selected. If only one β_{MQ} value yields acceptable results, that value is selected. If none of these values yields acceptable results, β_{MQ} is allowed to vary in the 90−130° range (the angle we call β_{MQ} has been found to be 108−112° in ref 3, 32−90° in ref 45, and 60−80° in ref 52). The digressions from β_{MQ} equal to 120 or 110.5° have been found in this study to be relatively small (see below).

Error Estimates. The errors in the best-fit MOMD parameters determined in this work are as follows: 3% in β_{MQ}, 10% in c_0^2 and c_2^2, and 15% in $R_\parallel$ and $R_\perp$.

3.2. Illustrative Simulations. Figure 4A shows ^2H line shapes obtained with c_0^2 = 2.0, c_2^2 = 3.5, β_{MQ} = 110.5°, and motional rates as depicted. Dynamic powder patterns similar to the red ($R_\perp = 0.79 \times 10^4$ s^{-1} and $R_\parallel = 6.31 \times 10^4$ s^{-1}) and black ($R_\perp = 0.79 \times 10^4$ s^{-1} and $R_\parallel = 63.1 \times 10^4$ s^{-1}) spectra are encountered in quite a few cases. These parameters belong to the predicted ranges. Dynamic powder patterns similar to the green and blue spectra, where $R_\perp = 3.16 \times 10^4$ s^{-1} is quite fast, are encountered rarely.

Figure 4B shows a set of dynamic ^2H powder patterns with c_0^2 = 2.2, $R_\perp = 1.6 \times 10^2$ s^{-1}, c_2^2, and $R_\parallel$ as depicted, and β_{MQ} varying from 90 to 130° in steps of 10° (see figure captions). Clearly, the ^2H line shapes are very sensitive to the rhombicity of the potential (c_2^2), the parallel diffusion rate ($R_\parallel$), and the local geometry (β_{MQ}).

The illustrative simulations presented in this section apply to deuterium nuclei executing axial local diffusion in a rhombic local potential. Specifics of the local motion, e.g., the relation of the local ordering/local diffusion frame to the local stereochemistry, are determined by the system investigated (see below).

3.3. MOMD Analysis of PS-Adsorbed LKα14 Peptide; $C-CD_3$ Dynamics. As pointed out above, ^2H line shapes from the peptide Ac-LKKLLKLLKKLLKL-OH (LKα14), deuterated selectively at various leucine positions with [*isopropyl*-$^2H_7$], have been used extensively to study physisorption onto biomineral surfaces (refs 4−6). The samples L5, L8, L11, and L14 adsorbed onto the apolar polystyrene (PS) surface have been investigated in ref 4 (the numbers denote the position of the isotope-labeled Leu residue in the peptide sequence). L8 has also been studied in its unbound (lyophilized) form, as well as adsorbed onto the polar surface of carboxyl-functionalized gold nanoparticles. The respective ^2H spectra are shown by the black traces in Figure 5A (see figure captions for specific designations). The spikes in the center of Figure 5Ab and Ac are associated with residual HDO; they should be ignored.

The red traces in Figure 5A represent the best-fit calculated spectra obtained in ref 4 with the following model. (1) The effective quadrupole constant, $\langle Q \rangle$, is allowed to vary. (2) Two-site methyl exchange with an angular separation of approximately 110° occurs. Its rate, k_{ex}, and the population ratio, p_1/p_2, are allowed to vary. (3) The instantaneous $C^\alpha-C^\beta$ bond executes equidistant jumps around its equilibrium orientation on the surface of a cone with a half-angle of 10°. The rate of this motion, k_{cone}, is allowed to vary. The contribution of the γ-deuteron is ignored in view of low signal intensity.

The experimental ^2H spectrum of the unbound peptide (Figure 5Aa) could not be reproduced satisfactorily with this model even when the cone half-angle was also allowed to vary, and the contribution of the γ-deuteron was accounted for.[5] The experimental ^2H spectra shown in Figure 5Ab−Af (black traces) have been reproduced very well (red traces).

The MOMD spectra that constitute best-fits to the experimental spectra of ref 5 (black traces in Figure 5A) are shown in Figure 5B. Spectra 5Bb and Be (L5 and L14 adsorbed onto PS) on the one hand, and spectra 5Bc and Bd (L8 and L11 adsorbed onto PS) on the other hand, are considered to be the same. MOMD reproduces well the experimental spectra, including the line shape shown in Figure 5Aa. The ^2H spectra of L5 and L14 have been reproduced with β_{MQ} = 120°, c_0^2 = 2.2, c_2^2 = 2.6, $R_\perp = 1.6 \times 10^2$ s^{-1}, and $R_\parallel = 2.0 \times 10^4$ s^{-1}. The ^2H spectra of L8 and L11 feature reduced potential strength (c_0^2 = 2.0 instead of 2.2), reduced potential rhombicity (c_2^2 = 2.2 instead of 2.6), and enhanced $R_\parallel$ (2.5×10^4 s^{-1} instead of 2.0×10^4 s^{-1}). β_{MQ} and $R_\perp$ are the same. The end-on view of the

DOI: 10.1021/acs.jpcb.5b07434
J. Phys. Chem. B 2015, 119, 14022−14032

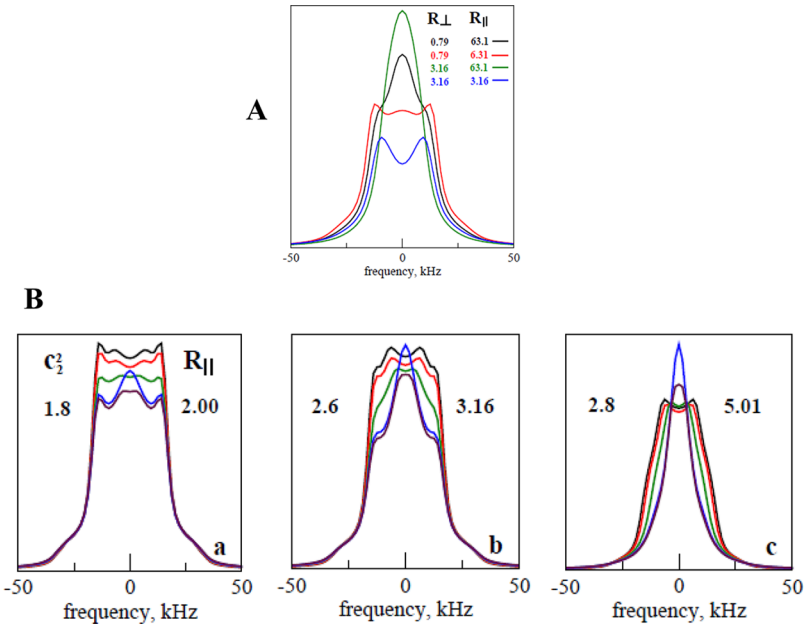

Figure 4. ^{2}H MOMD spectra obtained for $c_0^2 = 2.0$, $c_2^2 = 3.5$, $\beta_{MQ} = 110.5°$, and $R_\perp$ and $R_\parallel$ as depicted. The diffusion rates are given in units of 10^4 s^{-1} (part A). ^{2}H MOMD spectra obtained for $c_0^2 = 2.2$, $R_\perp = 0.016$ and (a) $c_2^2 = 1.8$ and $R_\parallel = 2.0$ in units of 10^4 s^{-1}; (b) $c_0^2 = 2.6$ and $R_\parallel = 3.16$ in units of 10^4 s^{-1}; and (c) $c_0^2 = 2.8$ and $R_\parallel$ in units of 10^4 s^{-1} (part B). In each panel, the various colors designate the value of β_{MQ} as follows: 90° (black), 100° (red), 110° (green), 120° (blue), and 130° (violet). Additional parameters used include $\langle Q \rangle = 52.8$ kHz and an intrinsic line width of 1 kHz.

helical structure of LKα14 depicted in ref 4 shows that L5 and L14 are relatively close to the PS surface whereas L8 and L11 are farther away from it. The MOMD description points to reduced spatial restrictions and enhanced motional rate, $R_\parallel$, for Leu side chains located farther from the PS surface.

Unbound L8 (Figure 5Ba) differs from PS-adsorbed L8 (Figure 5Bc). The potential form/symmetry changes upon adsorption, and the local diffusion becomes more axial (i.e., $R_\parallel/R_\perp$ becomes larger). As indicated above, the ^{2}H spectrum of unbound L8 (Figure 5Aa) could not be reproduced with the multimode models of refs 4 and 5. Allowing the local potential to be rhombic, and the local motion to be represented by a tensorial quantity, appears to be very important in this case.

The ^{2}H spectrum of L8 adsorbed onto carboxyl-functionalized gold nanoparticles (Figure 5Bf) was reproduced with $\beta_{MQ} = 110.5°$. It exhibits a potential form/symmetry that differs substantially from both its unbound form (Figure 5Ba) and its PS-adsorbed form (Figure 5Bc). The axiality of the local diffusion ($R_\parallel/R_\perp$) is similar for L8 adsorbed onto carboxyl-functionalized gold nanoparticles and L8 adsorbed onto PS. However, the absolute values differ, with both rates being twice slower for L8 adsorbed onto carboxyl-functionalized gold nanoparticles. The polarity, and in general the chemical nature, of the surface, is clearly an important factor in determining the structural dynamics of the Leu side chains. $R_\parallel$ is quite slow (1.3×10^4 s^{-1}) for both unbound L8 and L8 adsorbed onto carboxyl-functionalized gold nanoparticles; $R_\perp$ is substantially slower in the latter sample (8.0×10^2 s^{-1} versus 2.0×10^3 s^{-1}).

Thus, MOMD reproduces all of the experimental spectra shown by the black traces in Figure 5A, quantifying structural dynamics in terms of the form of the local potential, and the principal values and orientation of the local diffusion tensor. The three different forms of L8 are compared in terms of these qualifiers.

The black traces in Figure 6 represent experimental ^{2}H spectra acquired in ref 5 at room temperature (RT) from L1, L4, L5, L7, L8, L11, L12, and L14 adsorbed onto PS and from unbound L8 (the red traces represent the best-fit simulations from ref 5). We consider the spectra of L1, L4, L7, L8, and L11 on the one hand, and L5 and L14 on the other hand, to be the same.

The spectrum of L12 is similar to the spectrum of unbound L8. The authors of ref 5 also report sum frequency generation (SFG) experiments which yielded the orientation of the leucine side chains relative to the surface normal. Tilt angles of 30−48° for L4, L7, L8, and L11, 70° for L1, 68−74° for L5 and L14, and 82° for L12 have been determined with SFG. Except for L1 (the N-terminal residue of the peptide, which might act from the perspective of Leu side-chain dynamics more like residues farther away from the surface), the MOMD results are consistent with the SFG results. That is, small and large SFG-derived tilt angles correspond to different line shapes, and L12 is exceptional. All three groups are quantified in terms of potential form and diffusion tensor. Reference 5 has singled out only L12 as exceptional based on its outstandingly large cone half-angle (allowed to vary in ref 5) agreeing with a very large SFG-derived tilt angle.

The parameter combination used in ref 5 is different from the parameter combination used in ref 4. In ref 4, the parameters $\langle Q \rangle$, k_{ex}, p_1/p_2, and k_{cone} have been allowed to vary; the cone half-angle, θ, has been set equal to 10°, and the contribution of the γ-deuteron has been ignored. In ref 5, the parameters p_1/p_2, $\langle Q \rangle$, θ, and the percent contribution of the γ-deuteron have been allowed to vary; k_{ex} has been fixed at 6×10^6 s^{-1} and k_{cone} at 600 s^{-1}. In yet another study, L8 adsorbed onto PS and PS-COOH surfaces has been investigated as a function of temperature in the −40 to +60 °C range.[6] In that study, the parameters $\langle Q \rangle$, k_{cone}, and p_1/p_2 have been allowed to vary; k_{ex} has been fixed at 3×10^6 s^{-1}, the angle θ at 35°, and the contribution of the γ-deuteron at 16%. Within the scope of the analysis of ref 6, p_1 and p_2 exhibit different trends as a function of temperature for the PS-

DOI: 10.1021/acs.jpcb.5b07434
J. Phys. Chem. B 2015, 119, 14022−14032

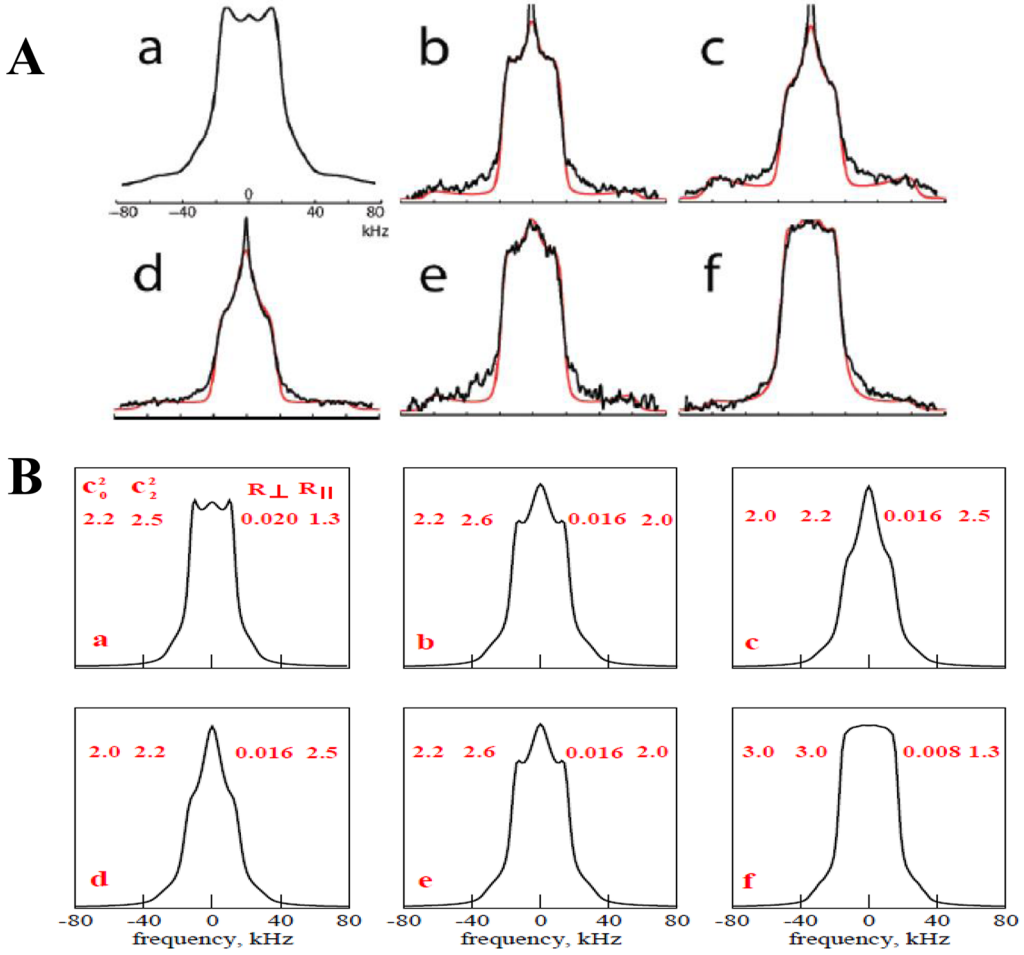

Figure 5. Experimental (black) and calculated (red) ^{2}H NMR line shapes of unbound LKα14 labeled with d_7-Leu at position 8 (L8) (a); PS-adsorbed L5 (b); PS-adsorbed L8 (c); PS-adsorbed L11 (d); and PS-adsorbed L14 (e). L8 adsorbed onto carboxyl-functionalized gold nanoparticles (f). Reproduced with permission from ref 4 (part A). ^{2}H MOMD spectra that reproduce the experimental line shapes of part A, obtained for β_{MQ} = 120° and the parameters depicted in the figure. The diffusion rates are given in units of 10^4 s^{-1}. Additional parameters used include $\langle Q \rangle$ = 52.8 kHz and an intrinsic line width of 1 kHz (part B, a–f).

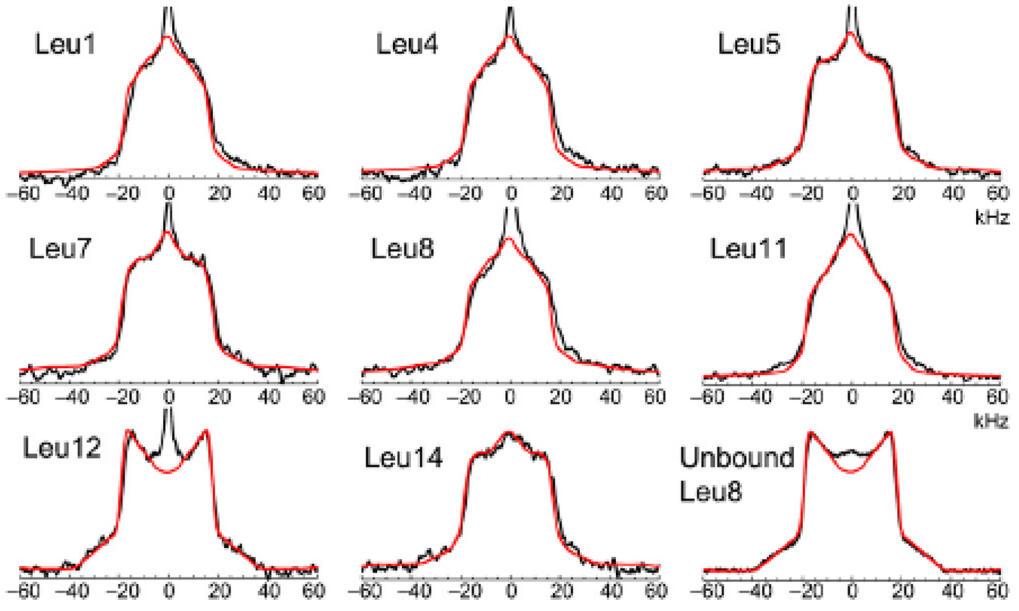

Figure 6. Experimental ^{2}H line shapes from L1, L4, L5, L7, L8, L11, L12, and L14 adsorbed onto a polystyrene surface and unbound L8 (black traces; the red traces represent the best-fit simulations from ref 5). Reproduced from ref 5. Copyright 2010 PNAS.

DOI: 10.1021/acs.jpcb.5b07434
J. Phys. Chem. B 2015, 119, 14022–14032

adsorbed and PS-COOH-adsorbed peptide. In particular, above 20 °C, p_1 and p_2 diverge for PS-adsorbed L8 and converge for PS-COOH-adsorbed L8. This has been interpreted in terms of p_1/p_2 being consistent with the Boltzmann relation $p_1/p_2 = \exp(-(E_2 - E_1)/k_BT)$ (where $E_2 - E_1$ is the energy difference between the site with population p_2 and the site with population p_1) for PS-COOH-adsorbed L8 but inconsistent for PS-adsorbed L8.

The analyses in refs 4, 5, and 6 differ in the identity of the fixed and allowed-to-vary parameters and the values of the fixed parameters. Taken separately, each scenario is plausible; taken together, ambiguities are encountered. Table 1 shows the

Table 1. Best-Fit Parameters Obtained for L8 Adsorbed onto the PS Surface at 20 °C in refs 4−6[a]

ref	$\langle Q \rangle$ (kHz)	k_{ex} (s^{-1})	k_{cone} (s^{-1})	p_1/p_2	$\theta°$	γ-deuteron
4	49	6×10^5	2×10^3	4/6	10*	
5	47	6×10^6 *	6×10^2 *	3.6/6.4	11	16%
6	46	3×10^6 *	6×10^2	3.6/6.4	35*	16%*

[a]Items designated by asterisks have been fixed in the respective calculations. The data of ref 6 have been obtained from ^{2}H spectra obtained under magic angle spinning (MAS).

results obtained for L8 adsorbed onto PS at 20 °C. Within the scope of the various analyses, k_{ex} varies by an order of magnitude, k_{cone} by a factor of 5, θ by a factor of 3.5, and the contribution of the γ-deuteron is zero in ref 4 and 16% in refs 5 and 6.

MOMD and the multimode models of refs 4−6 can only be compared in general terms. The MOMD model consists of a single dynamic mode comprised of a rhombic potential and an axial diffusion tensor. The multimode models of refs 4−6 are different versions of three independent simple dynamic modes comprising high-symmetry (scalar) parameters.

3.4. MOMD Analysis of Furanose Dynamics in *Hha*I Methyltransferase Target DNA; C−D Dynamics. Furanose dynamics in *Hha*I methyltransferase target DNA ^{2}H-labeled at the C2′ position have been studied with ^{2}H line shape analysis.[30] The experimental ^{2}H spectra of cytosines C6 and C8 in the DNA sequence are shown by the black traces in Figure 7Aa and Ab, respectively. The model utilized takes into account the global motion of the DNA and the (independent) local motion of the furanose ring. The global motion consists of jumps with rate k_{ex} on the surface of a cone with a half-angle of 20° centered at the helix axis.

The local motion is represented by C2′−^{2}H$_2$ moving with rate D rad^2/s in the presence of an axial potential with coefficient $\kappa\, k_BT$. The experimental ^{2}H spectra (black traces in Figure 7A) have been reproduced in ref 30 with $k_{ex} = 1.0 \times 10^4$ s^{-1}, $D = 1.8 \times 10^7$ rad^2/s, and $\kappa = 5\ k_BT$ (blue traces in Figure 7A).

Calculated MOMD spectra which constitute good fits to the experimental spectra of Figure 7A, and which reproduce the trend observed in going from C6 to C8, are shown in Figure 7Ba and Bb. For the C6 nucleotide, MOMD analysis yielded $c_0^2 = 2.1$, $c_2^2 = 3.0$, $R_\perp = 8.0 \times 10^2$ s^{-1}, $R_\parallel = 2.0 \times 10^4$ s^{-1}, and $\beta_{MQ} = 120°$. For C8, all the parameters except for c_0^2, which is equal to 2.2, are the same.

The experimental spectrum shown in Figure 7Ab differs from the experimental spectrum shown in Figure 7Aa in the intensity of the central "peak" relative to the intensity of the "horns".

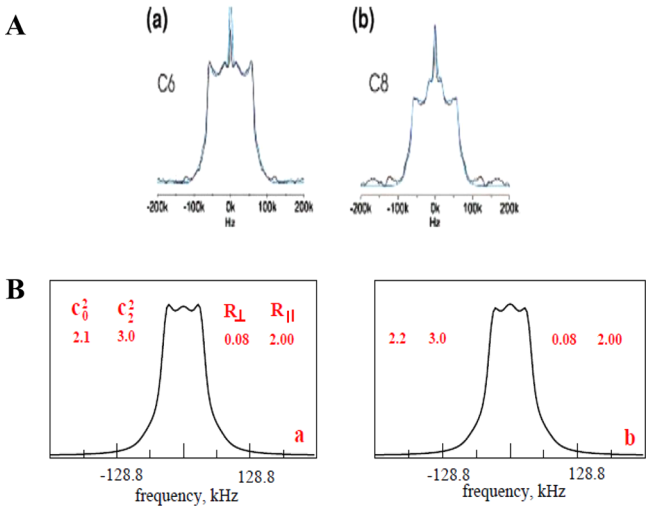

Figure 7. Experimental ^{2}H line shapes from the ^{2}H′ deuterons of the nucleotides C6 (a) and C8 (b) of the *Hha*I methyltransferase target DNA at a hydration level of 10% and 300 K. The calculated line shapes have been obtained as described in the text. Reproduced with permission from ref 30 (part A). ^{2}H MOMD spectra that reproduce the experimental line shapes of part A, obtained for $\beta_{MQ} = 120°$ and the parameters depicted in the figure. The diffusion rates are given in units of 10^4 s^{-1}. Additional parameters used include $Q = 170$ kHz and an intrinsic line width of 1 kHz (part B).

This feature could be reproduced by changing slightly the shape of the MOMD potential. Note that the spectrum shown in Figure 5Aa, which could not be reproduced with the models of refs 4 and 5, is similar to the spectrum shown in Figure 7Aa. Once again, our results highlight the fact that allowing the local potential to be rhombic is an important factor in rendering MOMD a general approach.

3.5. MOMD Analysis of Dimethyl-d_6 Ammonium Tetraphenylborate; N−CD_3 Dynamics. ^{2}H line shape (and relaxation) analysis has been used to study the dynamics of the ammonium cation, and a series of methylammonium cations, in their polycrystalline salts with tetraphenylborate.[44] These compounds are particularly interesting in view of the peculiar size and shape of the delocalized tetraphenylborate anion. Here we focus on $(CD_3)_2NH_2B(C_6H_5)_4$, for which temperature-dependent line shapes are given in ref 44. Figure 8A shows experimental spectra acquired at 245 (B), 270 (D), 275 (C), and 320 (A) K. Spectrum 8AB has been reproduced in ref 44 as a rigid-limit powder pattern with $\langle Q \rangle = 50$ kHz. Spectrum 8AA has been interpreted to result from methyl exchange between two sites with an angular change of 118.4°, and $\langle Q \rangle = 45.8$ kHz. Spectra 8AC and 8AD (and all of the spectra acquired between 250 and 300 K) have been interpreted as a superposition of spectra 8AA and 8AB, with temperature-dependent populations. It was concluded that there are temperature-dependent distributions of cations which do, and cations which do not, experience methyl exchange.

The compound $(CH_3)_2ND_2B(C_6H_5)_4$ has also been studied in ref 44. The ^{2}H spectrum obtained at 325 K has been reproduced with two-site exchange with an angular change of 103° (not shown).

MOMD reproduces the main features of the spectral evolution 8AB → 8AD → 8AC → 8AA within the scope of a single mode. The respective simulations are shown in Figure 8B. All of the line shapes in this figure have been obtained with $\beta_{MQ} = 109.5°$, which corresponds to methyl exchange between

DOI: 10.1021/acs.jpcb.5b07434
J. Phys. Chem. B 2015, 119, 14022−14032

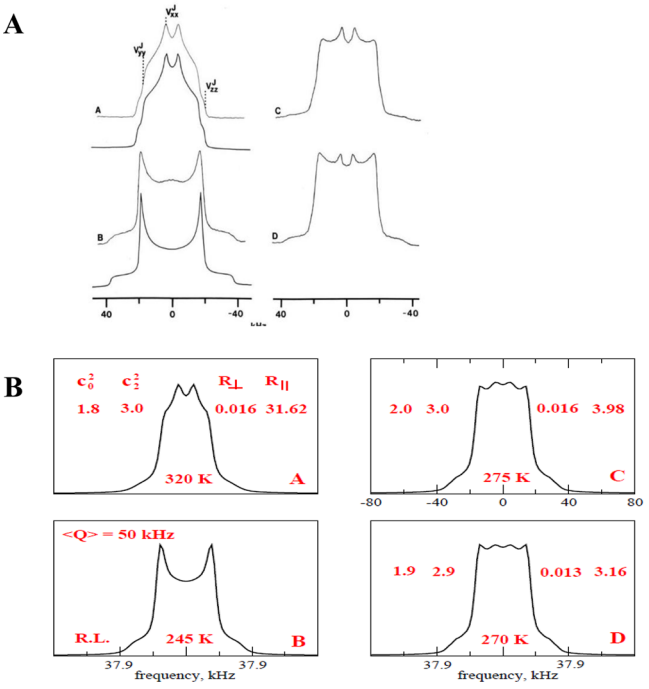

Figure 8. Experimental ^{2}H line shapes from dimethyl-d_6 ammonium tetraphenylborate acquired at 320 K (A), 245 K (B), 275 K (C), and 270 K (D). Spectrum B was simulated as a rigid-limit powder spectrum with $\langle Q \rangle$ = 50 kHz. Spectrum A was simulated with $\langle Q \rangle$ = 45.8 kHz and fast methyl exchange between two sites with an angular separation of 118.4°. Reproduced with permission from ref 44 (part A) Copyright 1990 Walter de Gruyter GmbH. ^{2}H MOMD spectra that reproduce the experimental line shapes of part a, obtained for β_{MQ} = 109.5° and the parameters depicted in the figure. The diffusion rates are given in units of 10^4 s^{-1}. Additional parameters used include $\langle Q \rangle$ = 50 kHz and an intrinsic line width of 1 kHz. For convenience, the experimental temperatures are also depicted (part B).

two corners of the positively charged nitrogen ion tetrahedron. For the 270 K spectrum, MOMD yielded a potential given by c_0^2 = 1.9 and c_2^2 = 2.9 and local diffusion given by $R_\perp = 1.3 \times 10^2$ s^{-1} and $R_\parallel = 3.16 \times 10^4$ s^{-1}. Increasing the temperature to 275 K implied a potential of a somewhat different form, and faster $R_\perp$ and $R_\parallel$. For the 320 K spectrum, MOMD yielded a further modified potential form, the same $R_\perp$ and substantially faster $R_\parallel$.

By plotting ln $R_\parallel$ as a function of $1/T$, we obtained an apparent activation energy of 8 ± 0.2 kcal/mol. Taking the ratio c_2^2/c_0^2 as a measure of rhombicity, one obtains 1.5, 1.5, and 1.7 at 270, 275, and 320 K, respectively. Larger potential rhombicity at higher temperature was encountered in our previous MOMD-based study of Leu side-chain dynamics in HP36.[43] We interpreted this finding in terms of two axial *structural* components contributing to the effective rhombic ordering tensor defined in terms of c_0^2 and c_2^2. At lower temperatures, one of these components partly "freezes out", rendering the effective ordering more axially symmetric. We offer this interpretation here as well.

The ^{2}H spectrum of $(CH_3)_2ND_2B(C_6H_5)_4$ at 325 K has been reproduced with MOMD employing the same parameters as those used to obtain Figure 8AA, except that $R_\parallel$ has been found to be equal to 1.0×10^5 s^{-1} instead of 3.2×10^5 s^{-1} (not shown).

3.6. MOMD Analysis of ^{2}H Line Shapes from Benzenehexa-6-hexanoate; C–D Dynamics. Benzene-*n*-alkanoates (where *n* represents the number of carbon atoms in the alkanoate chain) are compounds that exhibit extensive polymorphism in the solid state. The *n* = 6, 7, and 8 homologues have been studied previously with ^{13}C and ^{2}H line shape analysis, with the isotope labels applied at different molecular positions.[45] The various experimental spectra have been reproduced by superposing two-to-four rhombic powder patterns. Each rhombic spectrum has been interpreted as a motionally averaged spectrum ensuing from fast exchange between two side chain conformers. Exchange between rapidly exchanging pairs was considered to be slow. Temperature dependence has been interpreted to reflect changes in the relative population of the superposed rhombic spectra.

While most of the ^{2}H line shapes presented in ref 45 exhibit features typical of multicomponent spectra (e.g., multiple pairs of "shoulders", representing multiple "parallel" orientations in powder distributions), the phase III spectra of BHA6 ^{2}H-labeled at the β-carbon position (BHA6-βd_2) exhibit features consistent with a single dynamic mode (spectrum shape, in general, and dominant spectral features, in particular, that depend on the pulse separation in the quadrupole echo sequence[45] might emerge both from a single spectrum in the slow-motional regime, as well as from two superposed fast-motional spectra).

Figure 9A, left column, shows experimental spectra from BHA6-βd_2 acquired in phase IV at −46 °C and in phase III at −25, −12, and 13 °C. The phase IV spectrum has been reproduced as an isotropic powder pattern with 3/4×Q = 119 kHz. The phase III spectra have been interpreted in terms of two superposed rhombic powder patterns with temperature-dependent relative populations (Figure 9A, right column).

The experimental spectra shown in Figure 9A, left column, have been reproduced with MOMD in terms of a single dynamic mode characterized by rhombic local potential and axial local diffusion (Figure 9B). 3/4×Q = 119 kHz from the −46 °C phase IV spectrum has been used. The strength of the local potential, estimated by c_0^2, decreases with increasing temperature. The rhombicity of the potential, as evaluated by the ratio c_2^2/c_0^2, is 1.4, 1.4, and 1.7 at −25, −12, and 13 °C, respectively. We offered above a general qualitative interpretation to increasing potential rhombicity with increasing temperature: two axial contributions to the local structural restrictions at higher temperatures with one of them partly "freezing out" at lower temperatures. We offer this interpretation here as well.

The perpendicular motional rate, $R_\perp$, is relatively slow, however, with a sizable effect on the analysis. As expected, it increases with increasing temperature, ranging from 1.6×10^2 s^{-1} at −25 °C to 2.5×10^2 s^{-1} at 13 °C. An Arrhenius-type activation energy of 1.70 ± 0.24 kcal/mol has been calculated for it. $R_\parallel$ increases from 2.0×10^4 s^{-1} at −25 °C to 7.9×10^4 s^{-1} at 13 °C, and an Arrhenius-type activation energy of 5.05 ± 0.71 kcal/mol has been calculated for this component. The angle β_{MQ} was found to be 100.5, 112.5, and 120.5° at −25, −12, and 13 °C. This is the only example where the angle β_{MQ} had to be adjusted as a function of temperature. This might reflect changes in the nature of the axial contributions to the local spatial restrictions (see above), in addition to their temperature-dependence.

Thus, we found with MOMD analysis that the temperature-dependent spectra of BHA6-βd_2 in phase III can be interpreted in terms of a single dynamic mode (with small variations in the angle β_{MQ}). Motional rates, associated activation energies, and

DOI: 10.1021/acs.jpcb.5b07434
J. Phys. Chem. B 2015, 119, 14022−14032

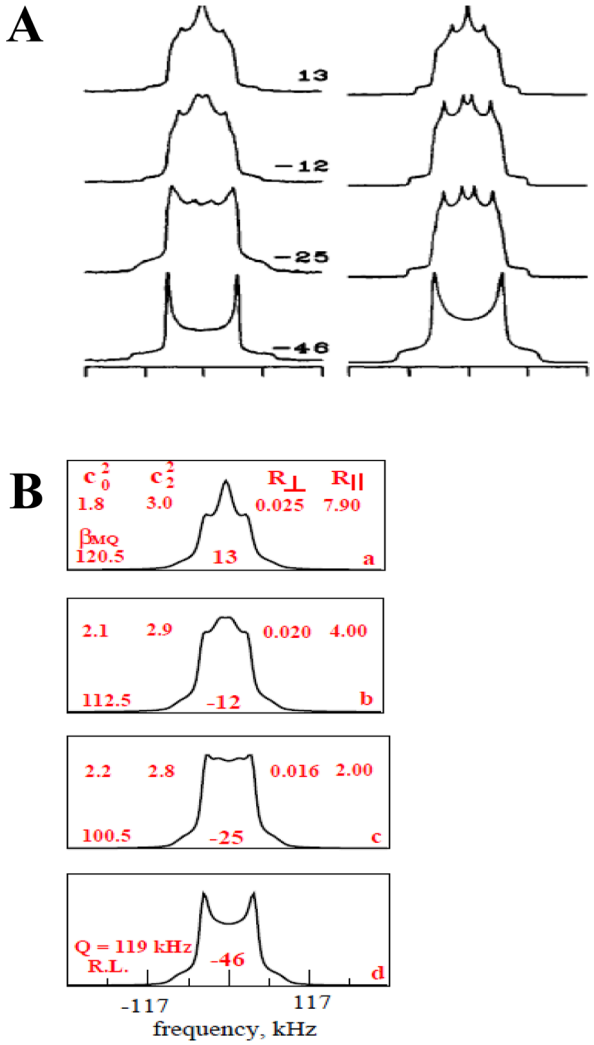

Figure 9. Experimental ^{2}H line shapes from BHA6-βd$_2$ in phase IV (−46 °C) and in phase III (−25, −12, and 13 °C) (upper left column). Calculated spectra obtained in ref 45 by superposing two rhombic powder patterns with temperature-dependent populations as delineated in the text (upper right column). Reproduced with permission from ref 45 (part A). ^{2}H MOMD spectra reproducing the experimental line shapes shown in part A, left column, obtained for the parameters depicted in the figure. They include the best-fit values of the potential coefficients c_0^2 and c_2^2; the best-fit values of the diffusion rates, $R_\perp$ and $R_\parallel$ given in units of 10^4 s^{-1}; and the fixed angles β_{MQ}. Additional parameters used include $3/4\times Q = 119$ kHz and an intrinsic line width of 1 kHz. For convenience, the experimental temperatures (in °C) are also depicted (part B).

the strength and rhombicity of the local potential at the ^{2}H-labeled sites were determined. This picture is to be compared with two independent exchange processes in their extreme motional narrowing limit, having temperature-dependent relative populations.

The following comments are in order. (1) We have treated in this study C−D, C−CD$_3$, and N−CD$_3$ dynamics. Within a good approximation (maximum deviation 9.5°), the main diffusion axes may be identified with relevant preceding chemical bonds. (2) The MOMD-based reproduction of some of the experimental spectra considered is not perfect. However, our objective has been to determine whether key features of dynamic ^{2}H line shapes from very different systems and experimental conditions can by reproduced reasonably well with the same set of general and physically relevant parameters. In general, this goal has been reached. Work aimed at improving the agreement between theory and experiment without overfitting the experimental data is in progress.

4. CONCLUSIONS

Quite a few systems (six in total) differing in nature have been subjected to MOMD analysis. In all of these cases, the local potential, given in units of k_BT, was found to be weak. Typical values of the axial coefficient, c_0^2, are 2.1−2.2. A particularly weak potential is associated with BHA6-βd$_2$ in phase III, where c_0^2 = 1.8 at 13 °C. This might indicate intermolecular interactions that are weaker than typically encountered in solids. The homologues BHA7 and BHA8 form a discotic phase at higher temperatures; our results suggest an inherent tendency of BHA6 to also do so.

For the C−CD$_3$ Leu probe, the axial potential coefficient, c_0^2, varies at room temperature from 2.0 to 2.2 for both HP36, and LKα14 adsorbed onto a PS surface. Thus, the strength of the local potential is similar for these two systems. On the other hand, the rhombic potential coefficient, c_2^2, varies from 2.0 to 3.4 for HP36 and from 2.2 to 2.6 for LKα14 adsorbed onto a PS surface. This is pointing to greater uniformity in the shape of the local potential at the Leu side chains of the surface-adsorbed peptide (note that we compare sets of four cases associated with HP36 with four cases associated with LKα14).

The furanose ring of *Hha*I methyltransferase target DNA, the methylammonium and dimethylammonium cations, and BHA6-βd$_2$ in phase III, exhibit relatively larger deviations of the local potential at the ^{2}H site from axiality as compared to HP36 and LKα14.

The diffusion rate, $R_\perp$, is generally small but not negligible. For the furanose ring of *Hha*I methyltransferase target DNA, $R_\perp$ is quite large (7.9×10^2 s^{-1}), in agreement with this outstandingly mobile structural element (cf. ref 30).

The diffusion rate $R_\parallel$ ranges from 1.3×10^4 to 7.9×10^4 s^{-1}. The methylammonium and dimethylammonium cations and BHA6-βd$_2$ in phase III exhibit relatively large $R_\parallel$ values. They also exhibit relatively large apparent activation energies: 8 ± 0.2 kcal/mol for the DMA cation and 5.05 ± 0.7 kcal/mol for BHA6-βd$_2$ in phase III.

Two experimental line shapes—the ^{2}H spectrum of Met73 in *Streptomyces* Subtilisin Inhibitor[41] and the ^{2}H spectrum of lyophilized LKα14 labeled at position 8 (see above)—could not be reproduced with the multi-simple-mode paradigm. They have been reproduced with MOMD.

The agreement between corresponding experimental and MOMD-derived ^{2}H line shapes can be improved in several ways. One could vary the angle α_{MQ} in addition to the angle β_{MQ}, include the L = 1 and L = 3 spherical harmonics in the expression for the local potential, and/or devise additional potential forms. All of these enhancements are associated with lowering the symmetry of the physical quantities entering the model. However, to fit such detailed models would require extensive sets of temperature-dependent ^{2}H spectra.

Prospects include the extension of MOMD so that it applies to ^{2}H spectra recorded under MAS (in progress), and developing MOMD for ^{15}N and ^{13}C nuclei. Concerted SRLS analysis of NMR relaxation in solution and MOMD analysis of NMR line shapes in the solid state for the same system is an important objective.

DOI: 10.1021/acs.jpcb.5b07434
J. Phys. Chem. B 2015, 119, 14022−14032

AUTHOR INFORMATION

Corresponding Authors

*E-mail: eva.meirovitch@biu.ac.il. Phone: 972-3-531-8049.
*E-mail: jhf3@cornell.edu. Phone: 1-607-255-3647.

Notes

The authors declare no competing financial interest.

ACKNOWLEDGMENTS

This work was supported by the Israel - U.S.A. Binational Science Foundation (Grant No. 2010185 to E.M. and J.H.F.) and the Israel Science Foundation (Grant No. 437/11 to E.M.). This work was also supported by NIH/NIGMS grant P41GM103521 to J.H.F.

REFERENCES

(1) Comellas, G.; Rienstra, C. Protein Structure Determination by Magic-Angle Spinning Solid-State NMR, and Insights into the Formation, Structure and Stability of Amyloid Fibrils. M. *Annu. Rev. Biophys.* **2013**, *42*, 515−536.

(2) McDermott, A. E. Structural and Dynamic Studies of Proteins by Solid-State NMR Spectroscopy: Rapid Movement Forward. *Curr. Opin. Struct. Biol.* **2004**, *14*, 554−561.

(3) Batchelder, L. S.; Sullivan, C. E.; Jelinski, L. W.; Torchia, D. A. Characterization of Leucine Side-Chain Reorientation in Collagen Fibrils by Solid-State ^{2}H NMR. *Proc. Natl. Acad. Sci. U. S. A.* **1982**, *79*, 386−389.

(4) Breen, N. F.; Weidner, T.; Li, K.; Castner, D. G.; Drobny, G. P. A Solid-State Deuterium NMR and Sum-Frequency Generation Study of the Side-Chain Dynamics of Peptides Adsorbed onto Surfaces. *J. Am. Chem. Soc.* **2009**, *131*, 14148−14149.

(5) Weidner, T.; Breen, T. F.; Li, K.; Drobny, G. P.; Castner, D. G. Sum Frequency Generation and Solid-State NMR Study of the Structure, Orientation and Dynamics of Polystyrene-Adsorbed Particles. *Proc. Natl. Acad. Sci. U. S. A.* **2010**, *107*, 13288−13293.

(6) Breen, N. F.; Li, K.; Olsen, G. L.; Drobny, G. P. Deuterium Magic Angle Spinning NMR Used to Study the Dynamics of Peptides Adsorbed onto Polystyrene and Functionalized Polystyrene Surfaces. *J. Phys. Chem. B* **2011**, *115*, 9452−9460.

(7) Abu-Baker, S.; Lu, J.-X.; Chu, S.; Brinn, C. C.; Makaroff, C. A.; Lorigan, G. A. Side-Chain and Backbone Dynamics of Phospholamban in Phospholipid Bilayers Utilizing ^{2}H and ^{15}N Solid-State NMR Spectroscopy. *Biochemistry* **2007**, *46*, 11695−11706.

(8) Chu, S.; Coey, A. T.; Lorigan, G. A. Solid-State ^{2}H and ^{15}N NMR Studies of Side-Chain and Backbone Dynamics of Phospholamban in Lipid Bilayers: Investigation of the N27A Mutation. *Biochim. Biophys. Acta, Biomembr.* **2010**, *1798*, 210−215.

(9) Long, J. R.; Mills, F. D.; Ganesh, O. K.; Antharam, V. C.; Farver, R. S. Partitioning, Dynamics, and Orientation of Lung Surfactant Peptide KL4 in Phospholipid Bilayers. *Biochim. Biophys. Acta, Biomembr.* **2010**, *1798*, 216−222.

(10) Vugmeyster, L.; Ostrovsky, D.; Ford, J. J.; Burton, S. D.; Lipton, A. S.; Hoatson, G. L.; Vold, R. L. Probing the Dynamics of a Protein Hydrophobic Core by Deuteron Solid-State Nuclear Magnetic Resonance Spectroscopy. *J. Am. Chem. Soc.* **2009**, *131*, 13651−13658.

(11) Vugmeyster, L.; Ostrovsky, D.; Khadjinova, A.; Elleden, J.; Hoatson, G. L.; Vold, R. L. Slow Motions in the Hydrophobic Core of Chicken Villin Headpiece Subdomain and their Contributions to Configurational Entropy and Heat Capacity from Solid-State Deuteron NMR Measurements. *Biochemistry* **2011**, *50*, 10637−10646.

(12) Seelig, J. Deuterium Magnetic Resonance: Theory and Application to Lipid Membranes. *Q. Rev. Biophys.* **1977**, *10*, 353−418.

(13) Davis, J. H. The Description of Membrane Lipid Conformation, Order and Dynamics by 2H-NMR. *Biochim. Biophys. Acta, Rev. Biomembr.* **1983**, *737*, 117−171.

(14) Wittebort, R. J.; Olejniczak, E. T.; Griffin, R. G. Analysis of Deuterium Nuclear Magnetic Resonance Line Shapes in Anisotropic Media. *J. Chem. Phys.* **1987**, *86*, 5411−5420.

(15) Keniry, M. A.; Rothgeb, M.; Smith, R. L.; Gutowsky, H. S.; Oldfield, E. Nuclear Magnetic Resonance Studies of Amino Acids and Proteins. Side-Chain Mobility of Methionine in the Crystalline Amino Acid and in Crystalline Sperm Whale (*Physester Catodon*) Myoglobin. *Biochemistry* **1983**, *22*, 1917−1926.

(16) Brown, M. F.; Heyn, M. P.; Job, C.; Kim, S.; Moltke, S.; Nakanishi, K.; Nevzorov, A. A.; Struts, A. V.; Salgado, G. F. J.; Wallat, I. Solid-State ^{2}H NMR Spectroscopy of Retinal Proteins in Aligned Membranes. *Biochim. Biophys. Acta, Biomembr.* **2007**, *1768*, 2979−3000.

(17) Rice, D.; Wittebort, R. J.; Griffin, R. G.; Meirovitch, E.; Stimson, E. R.; Meinwald, Y. C.; Freed, J. H.; Scheraga, H. A. Tyrosine Rotational Jumps in Crystalline Enkephalin: ^{2}H NMR Lineshapes for Aromatic Ring Motions in Solids. *J. Am. Chem. Soc.* **1981**, *103*, 7707.

(18) Cao, H.; Lin, G.; Jones, A. A. Deuterium Solid Echo Line Shape Study of Poly(ethylene oxide) Dynamics in a Blend with Poly(methyl methacrylate). *J. Polym. Sci., Part B: Polym. Phys.* **2005**, *43*, 2433−2444.

(19) Emsley, J. W.; Luckhurst, G. R.; Stockley, C. P. The Deuterium and proton-{deuterium} N.M.R. Spectra of the Partially Deuterated Nematic Liquid Crystal 4-n-pentyl-4′-cyanobiphenyl. *Mol. Phys.* **1981**, *44*, 565−580.

(20) Luz, Z.; Hewitt, S.; Meiboom, S. Deuterium Magnetic Resonance Studies of a Smectic Liquid Crystal. *J. Chem. Phys.* **1974**, *61*, 1758.

(21) Dong, R. Y. *Nuclear Magnetic Resonance of Liquid Crystals (Partially Ordered Systems)*; Springer-Verlag: New York, 1997.

(22) Spiess, H. W. In *Dynamic NMR spectroscopy*; Diehl, P., Fluck, E., Kosfeld, R., Eds.; Springer-Verlag: New York, 1978; Vol. *15*, pp 55−241.

(23) Torchia, D. A.; Szabo, A. Spin-Lattice Relaxation in Solids. *J. Magn. Reson.* **1982**, *49*, 107−121.

(24) Vold, R. R.; Vold, R. L. Deuterium Relaxation in Molecular Solids. *Adv. Magn. Opt. Reson.* **1991**, *16*, 85−171.

(25) Alam, T. M.; Drobny, G. P. Solid-State NMR Studies of DNA Structure and Dynamics. *Chem. Rev.* **1991**, *91*, 1545−1590.

(26) Campbell, R. F.; Meirovitch, E.; Freed, J. H. Slow Motional NMR Lineshapes of Very Anisotropic Rotational Diffusion: Phosphorus-31 NMR of Phospholipids. *J. Phys. Chem.* **1979**, *83*, 525.

(27) Meirovitch, E.; Freed, J. H. Slow Motional Lineshapes for Very Anisotropic Diffusion: I = 1 Nuclei. *Chem. Phys. Lett.* **1979**, *64*, 311.

(28) Schwartz, L. J.; Meirovitch, E.; Ripmeester, J. A.; Freed, J. H. A Quadrupole Echo Study of Internal Motions in Polycrystalline Media. *J. Phys. Chem.* **1983**, *87*, 4453−4461.

(29) Vold, R. L.; Hoatson, G. L. Effects of Jump Dynamics on Solid State Nuclear Magnetic Resonance Line Shapes and Spin Relaxation Times. *J. Magn. Reson.* **2009**, *198*, 57−72.

(30) Echodu, D.; Goobes, G.; Shajani, Z.; Pederson, K.; Meints, G.; Varani, G.; Drobny, G. P. Furanose Dynamics in the *Hha*I Methyltransferase Target DNA Studied by Solution and Solid-State NMR Relaxation. *J. Phys. Chem. B* **2008**, *112*, 13934−13944.

(31) Polnaszek, C. F.; Bruno, G. V.; Freed, J. H. ESR Lineshapes in the Slow-Motional Region: Anisotropic Liquids. *J. Chem. Phys.* **1973**, *58*, 3185−3199.

(32) Polnaszek, C. F.; Freed, J. H. Electron Spin Resonance Studies of Anisotropic Ordering, Spin Relaxation, and Slow Tumbling in Liquid Crystalline Solvents. *J. Phys. Chem.* **1975**, *79*, 2283−2306.

(33) Lin, W. J.; Freed, J. H. Electron Spin Resonance Studies of Anisotropic Ordering, Spin Relaxation, and Slow Tumbling in Liquid Crystalline Solvents: 3. Smectics. *J. Phys. Chem.* **1979**, *83*, 379−401.

(34) Misra, S. K.; Freed, J. H. In *Multifrequency electron paramagnetic resonance*; Misra, S. K., Ed.; Wiley-VCH: New York, 2011; Vol. *11*, pp 497−544.

(35) Schneider, D. J.; Freed, J. H. Spin relaxation and molecular dynamics. In *Advances in Chemical Physics*; Hirshfelder, J. O., Wyatt, R. E., Coalson, R. D., Eds.; John Wiley & Sons, Inc.: Hoboken, NJ, 1989; Vol. *73*, pp 387−528.

(36) Polimeno, A.; Freed, J. H. A Many-Body Stochastic Approach to Rotational Motions in Liquids. *Adv. Chem. Phys.* **1993**, *83*, 89−204.

DOI: 10.1021/acs.jpcb.5b07434
J. Phys. Chem. B 2015, 119, 14022−14032

(37) Polimeno, A.; Freed, J. H. Slow-Motional ESR in Complex Fluids: the Slowly Relaxing Local Structure Model of Solvent Cage Effects. *J. Phys. Chem.* **1995**, *99*, 10995−11006.
(38) Liang, Z.; Freed, J. H. An Assessment of the Applicability of Multifrequency ESR to Study the Complex Dynamics of Biomolecules. *J. Phys. Chem. B* **1999**, *103*, 6384−6396.
(39) Meirovitch, E.; Nayeem, A.; Freed, J. H. Protein-Lipid Interactions: a Single-Site Interpretation of the ESR Spectra. *J. Phys. Chem.* **1984**, *88*, 3454−3465.
(40) Dzikowski, B.; Freed, J. H. In *Nitroxides, Theory, Experiment and Applications*; Kokorin, A. I., Ed.; InTech: Rijrka, Croatia, 2012; pp 167−190.
(41) Zhang, Z.; Fleissner, M. R.; Tipikin, D. S.; Liang, Z.; Moscicki, J. K.; Earle, K. A.; Hubbell, W. L.; Freed, J. H. Multifrequency Electron Spin Resonance study of the Dynamics of Spin-Labeled T4 Lysozyme. *J. Phys. Chem. B* **2010**, *114*, 5503−5521.
(42) Liang, Z.; Freed, J. H.; Keyes, R. S.; Bobst, A. M. An Electron Spin Resonance Study of DNA Dynamics Using the Slowly Relaxing Local Structure Model. *J. Phys. Chem. B* **2000**, *104*, 5372−5381.
(43) Meirovitch, E.; Liang, Z.; Freed, J. H. Protein Dynamics in the Solid State from ^{2}H NMR Line Shape Analysis: a Consistent Perspective. *J. Phys. Chem. B* **2015**, *119*, 2857−2868.
(44) Gruwel, M. L. H.; Wasylishen, R. E. A Deuterium Study of Some Ammonium Tetraphenylborates. *Z. Naturforsch., A: Phys. Sci.* **1990**, *45a*, 55−66.
(45) Maliniak, A.; Greenbaum, S.; Poupko, R.; Zimmermann, H.; Luz, Z. Deuterium and Carbon-13 NMR of the Solid and Discotic Phases of Three Benzenehexa-n-alkanoates. *J. Phys. Chem.* **1993**, *97*, 4832−4840.
(46) Tugarinov, V.; Liang, Z.; Shapiro, Yu. E.; Freed, J. H.; Meirovitch, E. A Structural Mode-Coupling Approach to ^{15}N NMR Relaxation in Proteins. *J. Am. Chem. Soc.* **2001**, *123*, 3055−3063.
(47) Meirovitch, E.; Shapiro, Yu. E.; Polimeno, A.; Freed, J. H. Protein Dynamics from NMR: the SRLS Analysis Compared with MF Analysis. *J. Phys. Chem. A* **2006**, *110*, 8366−8396.
(48) Zerbetto, M.; Polimeno, A.; Meirovitch, E. A General and Efficient Theoretical/Computational Tool for Interpreting NMR Spin Relaxation in Proteins. *J. Phys. Chem. B* **2009**, *113*, 13613−13625.
(49) Meirovitch, E.; Shapiro, Yu. E.; Polimeno, A.; Freed, J. H. Structural Dynamics of Bio-Macromolecules by NMR: The Slowly Relaxing Local Structure Approach. *Prog. Nucl. Magn. Reson. Spectrosc.* **2010**, *56*, 360−405.
(50) Meirovitch, E.; Polimeno, A.; Freed, J. H. Protein Dynamics by NMR Spin Relaxation: The Slowly Relaxing Local Structure Perspective. In *Encyclopedia of Magnetic Resonance*; Harris, R. K., Wasylishen, R. E., Eds.; John Wiley: Chichester, U.K., 2011.
(51) Huang, T. H.; Skarjune, R. P.; Wittebort, R. J.; Griffin, R. G.; Oldfield, E. Restricted Rotational Isomerization in Polymethylene Chains. *J. Am. Chem. Soc.* **1980**, *102*, 7379−7381.
(52) Tamura, A.; Matsushita, M.; Naito, A.; Kojima, S.; Miura, K.-I.; Akasaka, K. Dynamics of the Three Methionyl Side Chains of *Streptomyces* Subtilisin Inhibitor. Deuterium NMR Studies in Solution and in the Solid-State. *Protein Sci.* **1996**, *5*, 127−139.

DOI: 10.1021/acs.jpcb.5b07434
J. Phys. Chem. B 2015, 119, 14022−14032